Progress: MRI Bias Field Correction Based on Tissue Labeling

Lianli Liu, Jiyang Chu*, Jie Li, Zhen Zeng
Electrical Engineering and Computer Science, University of Michigan.
Nuclear Engineering and Radiological Sciences, University of Michigan*.
Ann Arbor, MI 48109
{llliu,chujy,ljlijie,zengzhen}@umich.edu
EECS 556 Mar 28th 2014

I. Introduction

Intensity nonuniformities, also known as bias field in magnetic resonance imaging (MRI), arises from various factors such as imperfections in the radiofrequency (RF) pulse profile; nonuniform flip angles caused by an inhomogeneous transmit field; nonuniform reception sensitivity; RF penetration effects dependent upon the electromagnetic parameters of the object; wave behavior when the object size is equal to or more than one-half the wavelength of electromagnetic radiation and finally, gradient eddy currents related to the coupling between the object and gradient coils [1]. Such bias field manifests as a slowly varying signal intensity variation across tissue regions that should be uniform, as shown in Fig. 1. Human eyes are robust to such intensity inhomogeneity, thus medical experts can perform analysis tasks correctly. However, many intensity based image analysis algorithms are very sensitive to such intensity variation; thus correction of bias field is of great importance for accurate image analysis results.

Various methods have been proposed to address this issue, including prospective methods [2][3][4], where bias field is corrected during imaging, and retrospective ones, where bias field is estimated from images. Retrospective methods are more general in application as they do not rely on specific MR scanners and are able to remove patient induced inhomogeneity. Segmentation based method is one of important categories in retrospective methods.

However, most existing segmentation based methods only rely on image intensities or simple statistics referred from intensities [5][6][7]. Other potentially useful information, such as geometric shape, texture are ignored. The state of the art segmentation techniques developed in computer vision are deployed to obtain better segmentation results. In this project, we investigated different features for supervised based segmentations, and integrated the segmentation algorithm in bias field correction.

Specifically, our project includes the following parts

1) **Replication**: We will first reproduce existing work on segmentaion based bias field correction, as proposed by Chen et al.[8], as well as rich-feature segmentation method developed by Hoiem et al.[9].
2) **Extension**: After replication, we will integrate rich-feature segmentation technique into our bias filed correction framework to see if better segmentation techniques can lead to improvement in bias field correction.

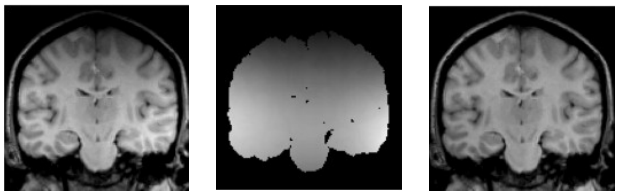

(a) Image corrupted by bias field (b) Estimated bias field (c) Corrected image

Figure 1. Bias field

The hypothesis we base our plan on are:

- Existing segmentation based bias field correction, can lead to approximate 15% improvement in segmentation accuracy, measured by the percentage of correctly classified voxels, as reported by Ahmed et al.[10]
- The rich feature tissue segmentation provides a more accurate segmentation than fuzzy c-means based segmentation methods. The quality of segmentation will be evaluated as the pixel-wise label accuracy, which can be measured against ground truth (human labeled or provided by synthetic data). We expect the segmentation accuracy to be 30% higher than fuzzy c-means [11].
- Integrating improved segmentation method with bias field correction will lead to higher segmentation accuracy compared with existing work[8] we replicate.we expect our performance to be improved by 30%.

II. Related Work

A. Segmentation Based Bias Field Correction

Among various retrospective methods, segmentation based methods have received much attention as they incorporate anatomy information, such as tissue type, into correction process. For example, maximum-likelihood (ML) or maximum a posteriori probability (MAP) criterion are applied to estimate image intensity probability distributions by parametric modes, where bias field is modeled as a Gaussian mixture model as in [12][13]. Fuzzy c-means based segmentation is also insensitively studied as it assigns partial membership to voxels, which is consistent with partial volume effect in MR images.

Standard fuzzy c-means objective function is modified in various ways to incorporate bias field effect [14][10][15]. Other methods based on non-parametric models are also proposed as in [16][17], using maxshift or meanshift clustering.

All these methods rely on image intensity only for segmentation, while over the past few decades, image segmentation has been an active area in computer vision, where numerous methods have been proposed that rely on more complicated features extracted from image instead of simple pixel intensity.

B. Image Segmentation

Image segmentation is the process of partitioning a digital image into multiple segments. The goal of segmentation is to simplify and/or change the representation of an image into something that is more meaningful and easier to analyze. It has long been investigated in the field of image processing and computer vision. Depending on whether prior information is provided, image segmentation can be categorized into unsupervised segmentation and supervised segmentation. Unsupervised segmentation clusters pixels based on their similarities in specific aspects (features). Examples of the specific aspects being used in computer vision community are color of a pixel, or richer features such as texture and shapes. Felzenszwalb [18] et al. proposed a graph-based algorithm to segment an image into regions. They start with a graph with each node corresponding to each pixel, and each pixel is connected to its neighbors by edges. Then they iteratively prune the edges if two connected components are dissimilar. The final graph with separated connected components correspond to separate regions in the segmentation result. Their work presented good segmentation results that align with the visual boundaries, but an image can be oversegmented in a sense that each segment does not correspond to a semantic entity, such as an object.

If we want to get semantic level segmentation, such as object segmentation, then prior knowledge on the object could be utilized for better segmentation. Supervised segmentation groups pixels into regions such that each region gets assigned to a specific pre-trained semantic label. These methods typically start with oversegmentation results of an image, and then learn a prior on the appearance for each semantic label, so that they can estimate the posterior probability of assigning a specific label to one segment based on the appearance of the segment. Hoiem et al. [9] learned the appearance model for some 3D geometric labels, such as "horizontal" and "vertical". Their method segments a given image into several geometric classes. The features that they used are simple and several 3D geometric features designed specifically for their task. In the case that hand crafted features are powerful enough, we can deploy deep learning [19] algorithm to automatically generate a hierarchy of useful features. Farabet et al. [19] used deep learning for generating a set of features in the task of scene labeling. The drawback of this line of work is the requirement of a huge amount of training data, which is hard to get due to the human efforts needed on labeling.

In this project we will investigate more deliberate segmentation methods for better bias field correction, as well as the corresponding regularization schemes to validate the above hypothesis.

III. Technical Approach

In this project, we plan to integrate rich feature tissue segmentation into the workflow of bias field correction, thus validate the hypothesis presented above. Therefore, existing work that we base our project on and plan to replicate are two-fold: 1) rich feature tissue segmentation; 2) segmentation based bias field correction.

A. Rich Feature Tissue Segmentation

We aim to segment a given MRI image into regions that correspond to 3 tissue classes, such as white matter, gray matter, and fluid. Appearance based features can be extracted to model each class. Integrating different features into a segmentation process is not a trivial task. Different features ask for different spatial support. Some are small-scale features like color or texture. Some are large-scale features like SIFT or SURF. How to provide the supporting area largely affects the robustness and accuracy of an segmentation algorithm. Inspired by the work of Hoiem et al. [9] scene labeling, we proposed to follow Hoiem's multi-level segmentation pipeline to segment tissues in MRI images.

As shown in Fig. 2, our proposed algorithm falls into 4 parts: 1) superpixel generation; 2) multiple hypothesis generation; 3) inference; 4) training.

1) Superpixel Generation: We directly apply the segmentation methods by Felzenszwalb [18] to get a set of over segmented superpixels. As shown in Fig. 2, the oversegmentation method also works with images with bias field. The goal of the tissue segmentation is to label each superpixel as one of the pre-defined tissue classes.

2) Multiple Hypothesis Generation: By changing the thresholds in the segmentation methods [18], we can have different oversegmentation results. It is intractable to evaluate every possible oversegmentation result and find the one that best segments the image into the pre-learned classes. Thus we will first group the superpixels of the oversegmentation into bigger regions based on some their features similarities. And the number of the final regions after the grouping can vary, thus we use different numbers of regions for different groupings of the regions, each referred as one of our hypothesis.

3) Inference: For each hypotheses, we assume that each region belong to the same tissue class, meaning all the superpixels within that region should be assigned to the same tissue label. Because of multiple hypothesis, each superpixel will be a member of several different regions from different hypothesis. The superpixel label confidence Eq. (1) is measured by a weighted sum of the label likelihoods of the regions that contain it, and the weights depend on the homogeneity likelihood of the regions [9]:

$$C(y_i = v|x) = \sum_{j}^{n_h} P(y_i = v|x, h_{ji}) P(h_{ji}|x) \qquad (1)$$

where y_i is the superpixel label, and v is one of the possible labels, and x is the image, n_h is the total number of hypothesis, and h_{ji} is the regions that contains the i^{th} superpixel for the j^{th} hypothesis, and y_j is the tissue label for the region h_{ji}. The label likelihood function of the regions, and the homogeneity

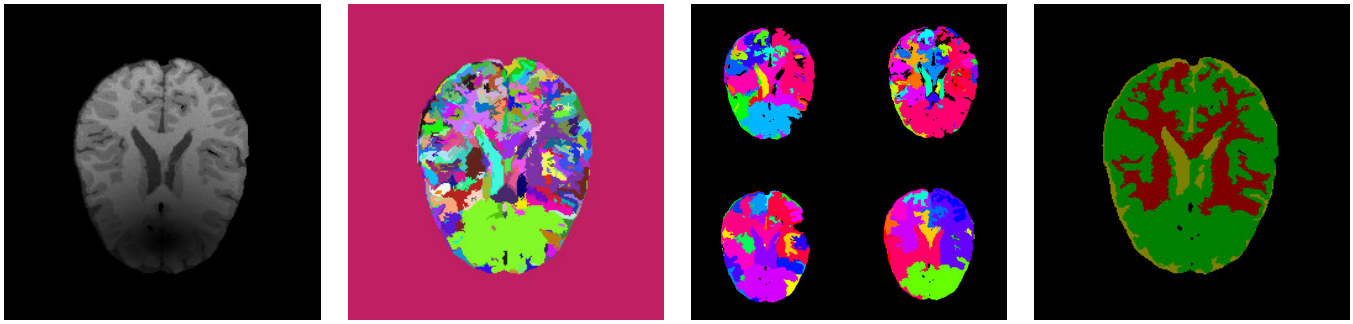

(a) Input Imaage (b) Over Segmentation (c) Multiple level Segments Hypothesis (d) Final Segmentation Result

Figure 2. Illustration figures for different steps in our proposed segmentation framework.

likelihood function of the regions are learned in our training stage, as explained below.

4) Training: In the training stage, for each training image, we generate multiple hypothesis. And for each hypothesis, we label the region as one of the pre-defined tissue class if the region corresponds well to one tissue class, or label the region as "mixed" if the region contains multiple tissue classes. Features are extracted within each region, and the features being used are as shown in Fig. 3. Details about features extractions are explained later. The label likelihood function of a region given the image data within that region is learned in a one versus rest fashion. And the homogeneity likelihood function of a region is learned by classifying homogeneously labeled (i.e. label as just one of the tissue classes) vs "mixed" labeled. Both likelihood functions can be estimated using logistic regression version of Adaboost [20], or using other classifiers such as SVM [21].

Features As shown in Fig. 3, we have several types of features that we can extract within each region. We chose this set of features since they can help recognize the tissue type as explained below.

Intensity: Different MRI image types (T1 weighted, T2 weighted, etc.) have different tissue contrast, and one single MRI volume may not be sufficient to separate all tissue types. For example, it has been reported that and T2-weighted images was more sensitive to bone density variation compared to other MRI image types; calculated fat image using Dixon method has strong contrast of fat with other tissue yet is not capable of separating other tissue types [22]. Most existing bias field uses single phase image (mainly T1 only) [23], thus it may be useful to study bias field correction using multi-phase images, utilizing characteristics of different MRI volume types. Here we represent the intensity using two intensity channels: T1, and T2, and calculate their mean (I1) and histograms (I2).

Texture: To explore whether texture gives us any cues for the tissue class, we extracted texture features and include them in the training stage. We apply a subset of the filter banks by Leung and Malik [24]. The texture is represented by the absolute filter response of each filter (X1) and the histogram of maximum responses over pixels within a segment (X2).

Location: Since MRI images using the same coil are mostly aligned together, the location is a very strong cue of what the tissue type is. The locations are represented by the normalized

Feature Description
Intensity
I1: T1 intensity
Texture
X1: LM filters: mean absolute response (15 filters)
X2: LM filters: histogram of maximum responses (15 bins)
Location
L1: normalized x and y, mean
L2: relative location to center point.
L3: relative distance to center point
Shape
S1: number of pixels in a superpixel
S2: normalized area in image
S3: ratio of width by height of a superpixel

Figure 3. Features to extract

pixel locations of the tissue type: the mean of the locations (L1), and also the 10th and 90th percentile of the pixel position of a region in the image (L2).

Shape: The shape and extension of the region is another cue that we can utilize. We represent the extension of the region by the number of superpixels (S1), and the shape is roughly represented by the normalized area in the image (S2). Depending on the results, we might incorporate more discriminative features for shape later.

B. Segmentation Based Bias Field Correction

The joint segmentation and bias field method proposed by Chen et al. [8] formulate the optimization problem the as

$$\begin{aligned} J(b,u) &= \sum_{i=1}^{c}\sum_{k=1}^{n} u_{ik}^{m}\|x_k - b_k - v_i\|^2 \\ \text{s.t. } &\sum_{i=1}^{c} u_{ik} = 1, \forall k \\ &0 \le u_{ik} \le 1, \forall k, i \end{aligned} \tag{2}$$

where x_k, b_k are log transformed image data and bias field at voxel k, u_{ik} is the fuzzy membership of voxel k belongs to tissue type i, c_i is the prototype vector of tissue class i and m controls the fuzzy degree.An iterative low pass filtering is applied to the estimated b after each iteration to guarantee smoothness.

This algorithm is computational expensive as an iterative 3D filtering is required at each algorithm iteration. Also, low pass filtering does not have a clear meaning in optimality nor do the authors specify which low pass filter is used in the paper.

To overcome this problem, instead of applying post processing step, we incorporate the constraint of smoothness into our optimization problem directly. This results in a Laplacian regularized problem

$$\begin{aligned} J(b,u) &= \sum_{i=1}^{c}\sum_{k=1}^{n} u_{ik}^{m}\|x_k - b_k - v_i\|^2 + \lambda\nabla\mathbf{b} \\ \text{s.t. } &\sum_{i=1}^{c} u_{ik} = 1, \forall k \\ &0 \le u_{ik} \le 1, \forall k, i \end{aligned} \tag{3}$$

Solving the above problem requires large matrix manipulation due to the data size of MR images. B-spline is the optimal solution for the regularized least square problem below

$$\hat{f} = \arg\min \frac{1}{n}\sum_{i=1}^{n}|y_i - f(t_i)|^2 + \beta\int |f^{(m)}(t)|^2 dt \tag{4}$$

Therefore, to reduce computation load, we first calculate bias field using Eq. (2), then we perform B spline smoothing to get the bias field.

Furthermore, we notice that although log transform is a necessary step to decouple multiplicative bias field and true MRI signal, it is not a linear operation and will distort the contrast of original image. Such contrast distortion will have negative impact on segmentation algorithm as it relies heavily on contrast between different tissue types.

Therefore, we replace Euclidean distance with a Gaussian distance on log transformed data, i.e $D(x,y) = 1 - exp(\frac{-\|x-y\|^2}{\sigma^2})$ to recover original image contrast.

To conclude, our algorithm operates as follows

1) Evaluate membership:

$$u_{ik} = \left(\frac{\lambda_k}{m}\right)^{\frac{1}{m-1}} \left(\frac{1}{D(x_k - \beta_k, v_i)}\right)^{\frac{1}{m-1}}$$

2) Update centroid:

$$v_i^* = \frac{\sum_{k=1}^{n} u_{ik}^m (1 - D(x_k\beta_k, v_i))(x_k - \beta_k)}{\sum_{k=1}^{n} u_{ik}^m (1 - D(x_k\beta_k, v_i))}$$

3) Calculate bias field:
$b_k^* =$

$$\left[x_k - \frac{\sum_{i=1}^{c} u_{ik}^m (1 - D(x_k - b_k, v_i))(x_k - v_i)}{\sum_{i=1}^{c} u_{ik}^m (1 - D(x_k - b_k, v_i))}\right]$$

4) Regularize bias field using B-spline smoothing
5) If the change of the updated centroid is smaller than a given threshold, terminate the algorithm and return results, else go back to step 1)

C. Integrate Segmentation into Bias Field Correction

Given the segmentation results in part A, bias field can be estimated based on the assumption that same tissue type have uniform intensity. At this stage, we are not confident that the segmentation algorithm described above is sensitive to intensity change or not. Therefore, we propose two strategy to incorporate segmentation into bias field correction, corresponding to the intensity-insensitive case and intensity-sensitive case.

Intensity Insensitive Case When segmentation is invariant to intensity change, bias field will have little impact on segmentation results. Thus we may rely on the segmentation results to generate a bias free image. Given the label of each voxel u_{ik} and the prototype of each voxel c_i (which can be easily obtained from training images or expert knowledge), the voxel intensity z_k bias free image will be

$$z_k = \sum_{i=1}^{c} u_{ik} c_i \tag{5}$$

With this bias free image, we can easily estimate bias field as

$$\mathbf{b} = \mathbf{X}/\mathbf{Z} \tag{6}$$

Where X is original image and Z is bias free image constructed by Eq. (6). However, the bias field estimation is an inverse problem and ill-posed. Therefore we apply the following regularized version, as proposed in [25]:

$$\hat{\mathbf{b}} = \arg\min \frac{1}{2}\|\mathbf{X} - \mathbf{Z}\mathbf{b}\|^2 + \frac{\lambda}{2}\|\mathbf{R}\mathbf{b}\|_2^2 \tag{7}$$

Where $\mathbf{R}$ is the finite differencing matrix to ensure the smoothness of estimated bias field. Following the algorithm proposed in [25], this problem can be solved efficiently using variable splitting and Augmented Lagrangian(AL) methods.

Intensity Sensitive Case Under this scenario, we cannot fully trust our segmentation results. Segmentation and bias correction have to be performed jointly for an optimal solution. To do this, we apply the fuzzy c-means version and define the following objective function

$$\begin{aligned} J(b,u) &= \sum_{i=1}^{c}\sum_{k=1}^{n} u_{ik}^{m}\|x_k - b_k - v_i\|^2 + R(\mathbf{b}) \\ \text{s.t. } &\sum_{i=1}^{c} u_{ik} = 1 \forall k \\ &0 \le u_{ik} \le 1, \forall k, i \end{aligned} \tag{8}$$

where b, u, c has the same meaning as in Eq. (2) Similar with Eq. (3), a regularization item $R(\mathbf{b})$ is introduced to enforce the smooth constraint on bias field. Implementation details on $R(\mathbf{b})$ will be discussed in the experiment section.

After segmentation, a bias field is estimated using Eq. (8) and the bias corrected image fed back into the segmentation algorithm to update u_{ik}.

IV. Experiment and Current Results

Our experiment consists of four parts: datasets, the evaluation of our replicated bias correction methods, the evaluation of our replicated rich-feature segmentation methods, and the evaluation of our segmentation methods integrated with our bias correction methods.

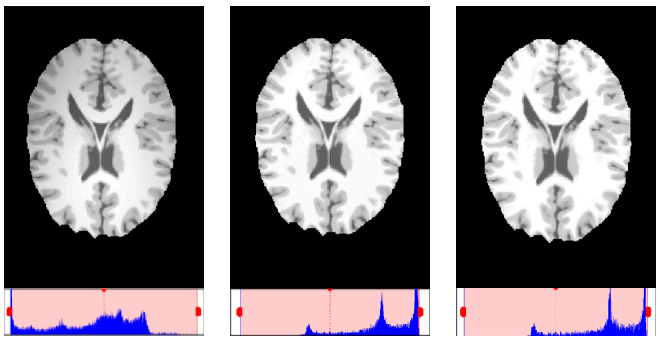

(a) T1 image corrupted by 80% bias field and and histogram histogram (b) Corrected T1 results and histogram (c) Ground truth T1 and histogram

Figure 4. IV-A1 T1 example.

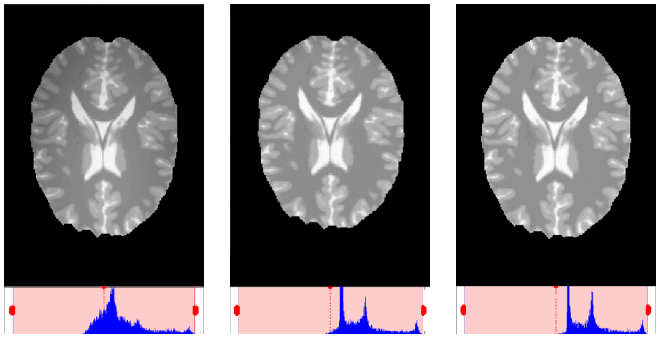

(a) T2 image corrupted by 80% bias field and and histogram histogram (b) Corrected T2 results and histogram (c) Ground truth T2 and histogram

Figure 5. IV-A1 T2 example.

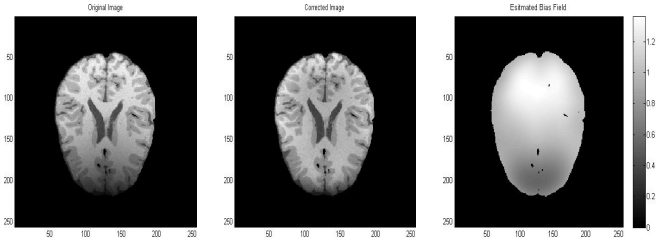

(a) Corrupted image (b) Corrected image (c) Estimated Bias Field

Figure 6. IV-A2 Artificial bias field applied and result.

A. Datasets

We used synthetic data downloaded from BrainWeb [26]. Two types of synthetic data are involved for tests:

1) T1-T2 Dataset: $217 \times 181 \times 181$ T1-weighted and T2-weighted images with bias field are included. The true bias field generated from real MRI scanners is provided on the website, thus gives the ground truth for bias field estimation. Specifically, the bias filed is at a strength of 80%. No ground truth labels of tissue classes are provided, thus this dataset is only used for bias field correction evaluations.

2) T1Label Dataset: T1-weighted images simulated from 20 brains anatomical model are included. The simulation images are bias free. Both hard tissue labels and soft classification results are provided, thus we used this dataset for segmentation evaluations. In addition, we augmented artificial bias field on this dataset for evaluations on our bias field correction method.

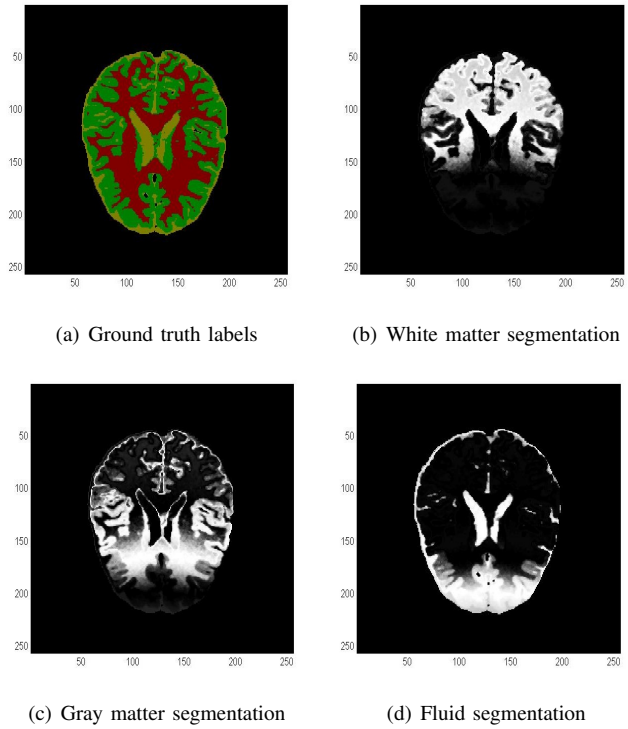

(a) Ground truth labels (b) White matter segmentation (c) Gray matter segmentation (d) Fluid segmentation

Figure 7. Before bias correction. Red: white matter; Greed: grey metter; Yellow: fluid.

B. Bias field estimation

Three tissue types within brain region are considered: white matter, gray matter and fluid. We tested our replications on IV-A1, and the MSE (mean square error) of the estimated bias field is 0.15. As shown in Fig. 4, the intensity histogram of the corrected T1 image is very similar to the intensity histogram of the ground truth image. We also show similar performance on T2 images in Fig. 5. These results validate that our replication is successful.

We also tested our replications on IV-A2, with images augmented by artificial bias field from Prof. Fessler's image reconstruction toolbox [27]. Parameter settings are the same with those in the tests on IV-A1. An example result is shown in Fig. 6. When the image is corrupted by a strong bias field, fuzzy c-means based segmentation without pre-correction of bias field suffers a lot as shown in Fig. 7. After we applied our bias field correction methods, the segmentation results of the corrected image is much better as shown in Fig. 8. Before the bias field correction, the average accuracy of fuzzy c-means segmentation is only 22%; after the bias field correction based on our replications, the accuracy at 31%.

C. Rich-feature segmentation

To evaluate the robustness and accuracy of our rich feature segmentation framework, we tested our algorithm on T1-weighted synthetic data in IV-A2. Artificial bias field is included using Prof. Fessler's tool box [27]. Given the ground truth labels of synthetic images, we evaluated the performance by averaging the label accuracy of each pixel. We compare our algorithm with fuzzy c-means method (FCM) and fuzzy c-means with bias field estimation (FCM-B). Currently, we

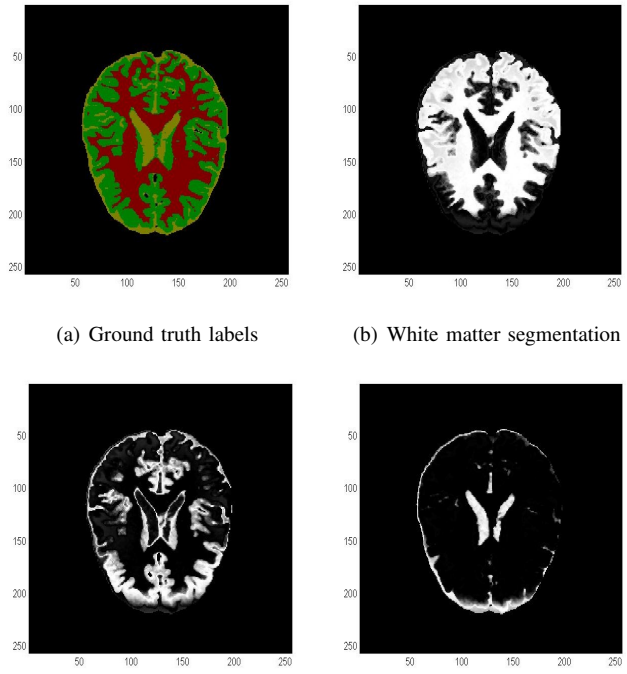

(a) Ground truth labels (b) White matter segmentation

(c) Gray matter segmentation (d) Fluid segmentation

Figure 8. After bias correction. Red: white matter; Greed: grey metter; Yellow: fluid.

Methods	Proposed	FCM	FCM-B
Average Accuracy	**72.6**%	22%	31%

Figure 9. Accuracy of segmentation. Proposed: our proposed rich-feature segmentation; FCM: cuzzy c-means segmentation without bias field estimation; FCM-B: fuzzy c-means segmatation with bias field estimation and B-spline regularization.

randomly picked 50 images as training data and the other 50 different images as testing data. Both training and testing sets have included bias field. Larger dataset will be considered in future experiments.

The experiment results are shown in Fig. 9. An instance in our test set is also shown in Fig. 10. The results demonstrate that our proposed rich-feature segmentation dramatically outperforms fuzzy c-means segmentation (by 50.6%), and even better than fuzzy c-means with bias field estimation (by 41.6%). The results fit our hypothesis. From the instance result Fig. 10, our method has shown its advantage in edge preservation. The main reason is that the edges are preserved in our over segmentation steps. In fuzzy c-means, edges are not considered explicitly. In the area that bias field is very strong, our method is not robust enough since over segmentation fail at those areas, as shown in Fig. 2(b). However, bias field estimation method is promising in those areas. A performance improvement can be expected once we combine our rich-feature segmentation and bias field estimation together.

D. Integrate rich-feature segmentation with bias field correction

To quantitively evaluate our bias field estimation and correction, we propose to use two different metrics: 1)intensity coded segmentation evaluation which is described by Vovk [23]; 2) intensity histogram distance between corrected image and original image without artificial bias field, where both histograms will be normalized to avoid uniform bias effect.

This part of experiment will be done after we combine our rich-feature segmentation and bias field estimation, as listed in V-B.

V. Summary

A. Encountered challenges

- For fuzzy c-means based methods, the most challenging part is the design of regularization scheme. Proper regularizer is required, otherwise the estimated bias field will be a residual image that compensates for segmentation error and violates its smooth varying property. We tested various methods including Gaussian low pass filtering, L_2 regularization, and finally decided that B-spline to be the best method.
- In segmentation part, feature selection is challenging. The reference work [9] we are based on, focusd on scene component segmentation. Those geometry features (e.g. horizon line) are totally useless in MRI images. We need to test many different combinations of different features or different forms of a single feature. Feature selection is accomplished by ablation study.
- Combination of rich-feature segmentation and bias field estimation is another difficulty we need to address, which is still under development. Since rich-feature segmentation cannot be explicitly involved into a cost optimation problem, a better optimization scheme needs to be explored.

B. Remaining steps

Up to this point, we have finished our replication part described in our project proposal, which corresponds to part A and part B in our method section. Fuzzy c-means based bias correction is implemented and achieves a 19% improvement over segmentation accuracy (31% vs. 22%) compared with plain fuzzy c-means segmentation, which is consistent with our first hypotheses. Rich feature segmentation is implemented on MRI data and is superior to fuzzy c-means based approach in terms of segmentation accuracy (79% vs. 31%), thus validates our second hypotheses. For future work, we will investigate the integration of rich-feature segmentation into bias field correction to see if it will lead to better performance, both in bias field estimation and segmentation, thus validate our third hypotheses. Implementation details include:

1) Implement the fusion framework integrating rich-feature segmentation into bias field correction.
2) Carry out experiments evaluate the performance of bias field correction.
3) Extend all the experiments on larger dataset. (Current testing set is onl 50 images.)
4) Evaluate the segmentation classifier over different pattern of bias field. (Current trainning set and testing set share the same bias field pattern.)
5) Intensively discuss the effect of different kinds of features in segmentation based on experiment.

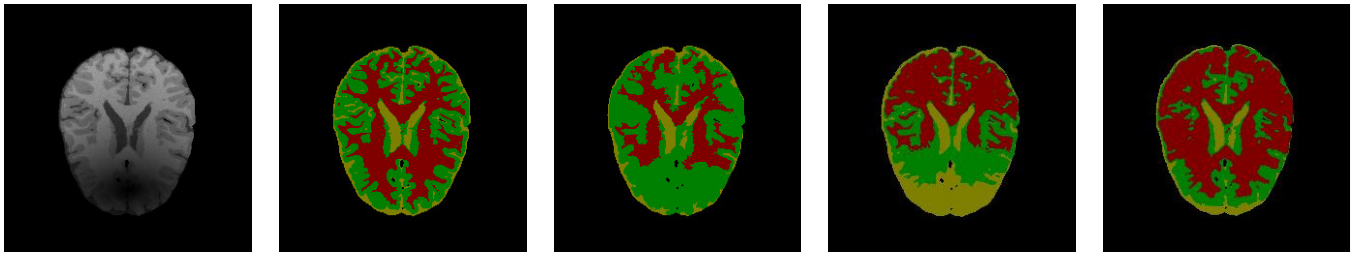

(a) Input: Image with Bias Field (b) Ground truth labels (c) Rich-feature Segmentation (d) FCM Segmentation (e) FCM-B Segmentation

Figure 10. An instance of segmentations results using different algorithms. Red: white matter; Greed: grey metter; Yellow: fluid.

REFERENCES

[1] J. Wang, M. Qiu, Q. X. Yang, M. B. Smith, and R. T. Constable, "Measurement and correction of transmitter and receiver induced nonuniformities in vivo," *Magnetic resonance in medicine*, vol. 53, no. 2, pp. 408–417, 2005.

[2] H. Watanabe, N. Takaya, and F. Mitsumori, "Non-uniformity correction of human brain imaging at high field by RF field mapping of B+ and B-," *Journal of Magnetic Resonance*, vol. 212, no. 2, pp. 426–430, 2011. http://www.sciencedirect.com/science/article/pii/S1090780711002588.

[3] H. Mihara, N. Iriguchi, and S. Ueno, "A method of rf inhomogeneity correction in mr imaging," *Magnetic Resonance Materials in Physics, Biology and Medicine*, vol. 7, no. 2, pp. 115–120, 1998. http://www.sciencedirect.com/science/article/pii/S1352866198000672.

[4] K. P. Pruessmann, M. Weiger, M. B. Scheidegger, P. Boesiger, *et al.*, "Sense: sensitivity encoding for fast mri," *Magnetic resonance in medicine*, vol. 42, no. 5, pp. 952–962, 1999. http://macduff.usc.edu/ee591/library/Pruessmann-SENSE.pdf.

[5] M. Styner, C. Brechbuhler, G. Szckely, and G. Gerig, "Parametric estimate of intensity inhomogeneities applied to MRI," *Medical Imaging, IEEE Transactions on*, vol. 19, no. 3, pp. 153–165, 2000. http://ieeexplore.ieee.org/xpls/abs_all.jsp?arnumber=845174.

[6] J. G. Sled, A. P. Zijdenbos, and A. C. Evans, "A nonparametric method for automatic correction of intensity nonuniformity in MRI data," *Medical Imaging, IEEE Transactions on*, vol. 17, no. 1, pp. 87–97, 1998. http://ieeexplore.ieee.org/xpls/abs_all.jsp?arnumber=668698.

[7] N. J. Tustison, B. B. Avants, P. A. Cook, Y. Zheng, A. Egan, P. A. Yushkevich, and J. C. Gee, "N4itk: improved n3 bias correction," *Medical Imaging, IEEE Transactions on*, vol. 29, no. 6, pp. 1310–1320, 2010. http://www.ncbi.nlm.nih.gov/pubmed/20378467.

[8] W. Chen and M. L. Giger, "A fuzzy c-means (fcm) based algorithm for intensity inhomogeneity correction and segmentation of mr images," in *Biomedical Imaging: Nano to Macro, 2004. IEEE International Symposium on*, pp. 1307–1310, IEEE, 2004. http://ieeexplore.ieee.org/xpls/abs_all.jsp?arnumber=1398786.

[9] D. Hoiem, A. A. Efros, and M. Hebert, "Geometric context from a single image," in *Computer Vision, 2005. ICCV 2005. Tenth IEEE International Conference on*, vol. 1, pp. 654–661, IEEE, 2005. http://ieeexplore.ieee.org/xpls/abs_all.jsp?arnumber=1541316&tag=1.

[10] M. N. Ahmed, S. M. Yamany, N. Mohamed, A. A. Farag, and T. Moriarty, "A modified fuzzy c-means algorithm for bias field estimation and segmentation of mri data," *Medical Imaging, IEEE Transactions on*, vol. 21, no. 3, pp. 193–199, 2002. http://ieeexplore.ieee.org/xpls/abs_all.jsp?arnumber=996338.

[11] S. Chen and D. Zhang, "Robust image segmentation using fcm with spatial constraints based on new kernel-induced distance measure," *Systems, Man, and Cybernetics, Part B: Cybernetics, IEEE Transactions on*, vol. 34, no. 4, pp. 1907–1916, 2004. http://ieeexplore.ieee.org/xpls/abs_all.jsp?arnumber=1315771.

[12] W. M. Wells III, W. E. L. Grimson, R. Kikinis, and F. A. Jolesz, "Adaptive segmentation of mri data," *Medical Imaging, IEEE Transactions on*, vol. 15, no. 4, pp. 429–442, 1996.

[13] A. H. Andersen, Z. Zhang, M. J. Avison, and D. M. Gash, "Automated segmentation of multispectral brain mr images," *Journal of neuroscience methods*, vol. 122, no. 1, pp. 13–23, 2002. http://ieeexplore.ieee.org/xpls/abs_all.jsp?arnumber=511747.

[14] M. N. Ahmed, S. M. Yamany, A. A. Farag, and T. Moriarty, "Bias field estimation and adaptive segmentation of mri data using a modified fuzzy c-means algorithm," in *Computer Vision and Pattern Recognition, 1999. IEEE Computer Society Conference on.*, vol. 1, IEEE, 1999. http://ieeexplore.ieee.org/xpls/abs_all.jsp?arnumber=786947.

[15] D. L. Pham and J. L. Prince, "An adaptive fuzzy c-means algorithm for image segmentation in the presence of intensity inhomogeneities," *Pattern Recognition Letters*, vol. 20, no. 1, pp. 57–68, 1999. http://www.sciencedirect.com/science/article/pii/S0167865598001214.

[16] B. Likar, J. Derganc, and F. Pernus, "Segmentation-based retrospective correction of intensity nonuniformity in multispectral mr images," in *Medical Imaging 2002*, pp. 1531–1540, International Society for Optics and Photonics, 2002. http://www.sciencedirect.com/science/article/pii/S0167865598001214.

[17] J. Derganc, B. Likar, and F. Pernus, "Nonparametric segmentation of multispectral mr images incorporating spatial and intensity information," in *Medical Imaging 2002*, pp. 391–400, International Society for Optics and Photonics, 2002. http://proceedings.spiedigitallibrary.org/proceeding.aspx?articleid=879732.

[18] P. F. Felzenszwalb and D. P. Huttenlocher, "Efficient graph-based image segmentation," *International Journal of Computer Vision*, vol. 59, no. 2, pp. 167–181, 2004. http://www.cs.cornell.edu/~dph/papers/seg-ijcv.pdf.

[19] C. Farabet, C. Couprie, L. Najman, and Y. LeCun, "Learning hierarchical features for scene labeling," *Pattern Analysis and Machine Intelligence, IEEE Transactions on*, vol. 35, no. 8, pp. 1915–1929, 2013. http://ieeexplore.ieee.org/xpl/articleDetails.jsp?arnumber=6338939.

[20] M. Collins, R. E. Schapire, and Y. Singer, "Logistic regression, adaboost and bregman distances," *Machine Learning*, vol. 48, no. 1-3, pp. 253–285, 2002. http://link.springer.com/article/10.1023/A:1013912006537.

[21] C. Cortes and V. Vapnik, "Support-vector networks," *Machine learning*, vol. 20, no. 3, pp. 273–297, 1995. http://link.springer.com/article/10.1007/BF00994018.

[22] S.-H. Hsu, Y. Cao, K. Huang, M. Feng, and J. M. Balter, "Investigation of a method for generating synthetic ct models from mri scans of the head and neck for radiation therapy," *Physics in medicine and biology*, vol. 58, no. 23, p. 8419, 2013. http://www.ncbi.nlm.nih.gov/pubmed/24217183.

[23] U. Vovk, F. Pernus, and B. Likar, "A review of methods for correction of intensity inhomogeneity in mri," *Medical Imaging, IEEE Transactions on*, vol. 26, no. 3, pp. 405–421, 2007. http://ieeexplore.ieee.org/xpls/abs_all.jsp?arnumber=4114560.

[24] T. Leung and J. Malik, "Representing and recognizing the visual appearance of materials using three-dimensional textons," *International Journal of Computer Vision*, vol. 43, no. 1, pp. 29–44, 2001. http://link.springer.com/article/10.1023/A:1011126920638.

[25] M. J. Allison, S. Ramani, and J. A. Fessler, "Accelerated regularized estimation of mr coil sensitivities using augmented lagrangian methods," *Medical Imaging, IEEE Transactions on*, vol. 32, no. 3, pp. 556–564, 2013. http://ieeexplore.ieee.org/xpls/abs_all.jsp?arnumber=6361300.

[26] B. Aubert-Broche, A. C. Evans, and L. Collins, "A new improved version of the realistic digital brain phantom," *NeuroImage*, vol. 32, no. 1, pp. 138–145, 2006. http://brainweb.bic.mni.mcgill.ca/brainweb/.

[27] J. A. Fessler, "Image reconstruction toolbox," http://web.eecs.umich.edu/~fessler/code/index.html.